Upper Miocene volcanic ash layers from central Italy: tracking down the volcanic source

Query Details

1. Please check affiliations if captured/presented correctly.

ok

2. Please check supplementary if captured/presented correctly.

ok

3. Please check section headings are assigned to appropriate headings.

ok

4. Please check figures if captured/presented correctly.

ok

5. Please check captured formal para if correct.

ok

6. Michon and Merle 2001 has been changed to Michon and Merle, 2000 so that this citation matches the Reference List. Please confirm that this is correct.

ok

7. Savelli 1987 has been changed to Savelli, 1988 so that this citation matches the Reference List. Please confirm that this is correct.

ok

8. Please check tables if captured/presented co rrectly.

ok

9. Eggleton and Banfield 1980 has been changed to Eggleton and Banfield, 1985 so that this citation matches the Reference List. Please confirm that this is correct.

ok

10. Please check if back matter statements are captured correctly.

ok. I added a sentence in the Acknowledgements

Research Article

Upper Miocene volcanic ash layers from central Italy: tracking down the volcanic source

Matteo Roverato ✉
Email : matteo.roverato@unibo.it
Affiliationids : Aff1 Aff2, Correspondingaffiliationid : Aff1
Federico Farina Affiliationids : Aff3
Matteo Lupi Affiliationids : Aff2
Maria Ovtcharova Affiliationids : Aff2
Alessandro Montanari Affiliationids : Aff4
Marco Bonini Affiliationids : Aff5
Domenico Montanari Affiliationids : Aff5

Aff1 Department Bigea, Alma Mater Studiorum, University of Bologna, Piazza Di Porta San Donato 1, 46100, Bologna, Italy

Aff2 Department of Earth Sciences, University of Geneva, Geneva, Switzerland

Aff3 Department of Earth Sciences “Ardito Desio”, University of Milan, Milan, Italy

Aff4 Osservatorio Geologico Di Coldigioco, Cda. Coldigioco 4, 62021, Apiro, Italy

Aff5 Institute of Geosciences and Earth Resources, CNR, Florence, Italy

Received: 3 June 2024 / Accepted: 19 September 2024

Abstract

The Mediterranean region has AQ1 been characterized by intense explosive volcanism since the Eocene. These eruptions ejected tephra, including fine-grained ash, which were thrown into the air and dispersed over wide areas to later be deposited as ash layers, many of which are preserved in some continental and marine sedimentary basins. Their study provides crucial insights into past volcanic activity, yet, for many of such ash layers, the understanding of their sources remains challenging. The presence of many ash layers across central Italy is widely recognized in literature although not uniquely associated with a specific volcanic source. We investigate in detail upper Tortonian (~ 7.6 Ma) ash layers sampled from three different localities, from the Tyrrhenian to the Adriatic coast of Italy, comparing our results with others already described in the literature. Electron microprobe geochemical analyses on biotite crystals, U–Pb ID-TIMS and LA-ICP-MS geochronological dating, and trace elements/Lu–Hf isotope analyses on zircons permitted us to expand our knowledge of these ancient ash deposits. Several potential volcanic centers were active during the late Tortonian, including the Massif Central (France), the Valencia trough (Spain), the Betics-Rif orogen (Spain-Morocco), and eastern Carpathians (Romania) and Capraia island (Italy). Through detailed radioisotopic dating and geochemical comparisons, we narrow down the possible source to the Upper Miocene Capraia island volcano (Tuscan archipelago), located in the northern Tyrrhenian basin.

Keywords

Ash layers
Mediterranean volcanism
Capraia Island
Tephrochronology
Geochronology
Geochemistry

Editorial responsibility: Editorial responsibility: J. Smellie

Supplementary Information AQ2

The online version contains supplementary material available at https://doi.org/10.1007/s00445-024-01774-0 .

Introduction

Explosive volcanic eruptions AQ3 produce tephra that are ejected into the atmosphere and are dispersed by the prevailing winds blanketing the topography as either continuous or discontinuous layers of ash. They are erupted over very short time spans, geologically speaking, typically from hours to a few months and could travel for several hundreds kilometers. These ash layers allow linking and synchronizing eruptive records across different geological domains in space and time. Such geological relationships are constrained by radiometric, incremental, or other methods known as tephrochronology (Lowe et al. 2011). Tephra layers preserved in distal reaches also enhance our understanding of the volcanic history of a region, since proximal volcanic successions often record only the most recent or volumetrically most relevant part of the explosive history of a volcano (Leicher et al. 2019).

The intense explosive volcanism that characterized the Mediterranean regions since the Eocene led to the deposition of several volcaniclastic ash layers (e.g., Montanari et al. 2017 and references therein; Narcisi & Vezzoli 1999 and references therein). During this period, the geodynamic and paleo-geographic settings of this region were complex, and the range of tectonic and magmatic/volcanic processes such as continental rifting and drifting, back-arc basin opening, and formation of orogens and volcanic arcs, created an intricate variety of geo-environments (Lustrino et al. 2011). Hence, the reconstruction of the volcanic evolution and provenances of volcanic tephras in such a relatively small region is challenging, and most of the studies focused on well-preserved Quaternary volcaniclastic deposits (e.g., Giaccio et al. 2013; Marra et al. 2014). In the Mediterranean regions, studies concerning pyroclastic layers older than 200 ka are scarce and fragmentary due to the sparse occurrence of well-preserved deposits (Münch et al. 2005). Moreover, various eruption sources were active at the same time representing multiple candidates for any given volcanic ash layer.

To shed light into the Upper Miocene volcanic activity of the region, we identify and investigated biotite-rich tephra layers from three stratigraphic sections spread across central Italy related to the upper Tortonian time interval. We combine field, geochronological, and geochemical investigations to provide a chrono- and chemo-stratigraphic framework of the volcanic activity. We investigate the geochemical and geochronological characteristics of the studied ash layers and compare them to others already described in the literature, which are no longer traceable mainly due to man-made processes. Although in the Northern and Central Apennines, several volcanogenic layers interbedded in different stratigraphic intervals within Neogene terrestrial, and marine deposits have been previously described (D’Orazio et al. 1995; Krijgsman et al. 1997; Rook et al. 2000; Aldinucci et al. 2005; Trua et al. 2010); none of those studies have uniquely identified the volcanic sources that produced these deposits. The aim of our study is to describe and characterize these upper-

Tortonian ash layers to assess whether they belong to one or more eruptive centers. We also attempt to identify the approximate geographic origin(s) of the eruptive center(s) by comparing ages and geochemical fingerprints with published analyses derived from all potential source volcanoes.

Upper Tortonian tephra layers in central Italy

During the Late Miocene sub-Epoch, the peri-Tyrrhenian region was affected by the orogenic activity in the axial portion of the uplifting northern Apennines and the opening of the Tyrrhenian Sea (Martini et al. 2001). Shallow basins, characterized by the deposition of fluvio-lacustrine to marine sediments, developed on the western side of the uprising northern Apennines chain. On the eastern side of the Apennines, the region was also characterized by eastward migrating foredeep depocenters (Manzi et al. 2005). Oligo-Miocene deep-water turbiditic successions were deposited in the recently formed basins (Trua et al. 2010). Along the eastern coastline of Central Italy, the deposition remained mainly pelagic throughout most of the Miocene due to its external position relative to the Apennine orogenic front (Hüsing et al. 2009). Scattered across the basins of Central Italy, it is possible to identify distinct upper Tortonian volcanic ash layers (Fig. 1 a) that are characterized by the abundant occurrence of biotite flakes. These distinctive layers, described in the literature, are reported below from the West to the East.

Fig. 1

a Simplified geological map of central **AQ4** Italy showing the location of the layers analyzed in the present work (white dots—PAS, CAS, MdC)) and those from the literature (black dots—FAL, PEG, PTR). **b** Sketch map of the Mediterranean region representing all the magmatic/volcanic centers of all composition (calc-alkaline, alkaline, and shoshonitic) active during the late-Tortonian (modified after Trua et al. 2010); CVP, Calatrava Volcanic Province, CVZ. Catalan Volcanic Zone

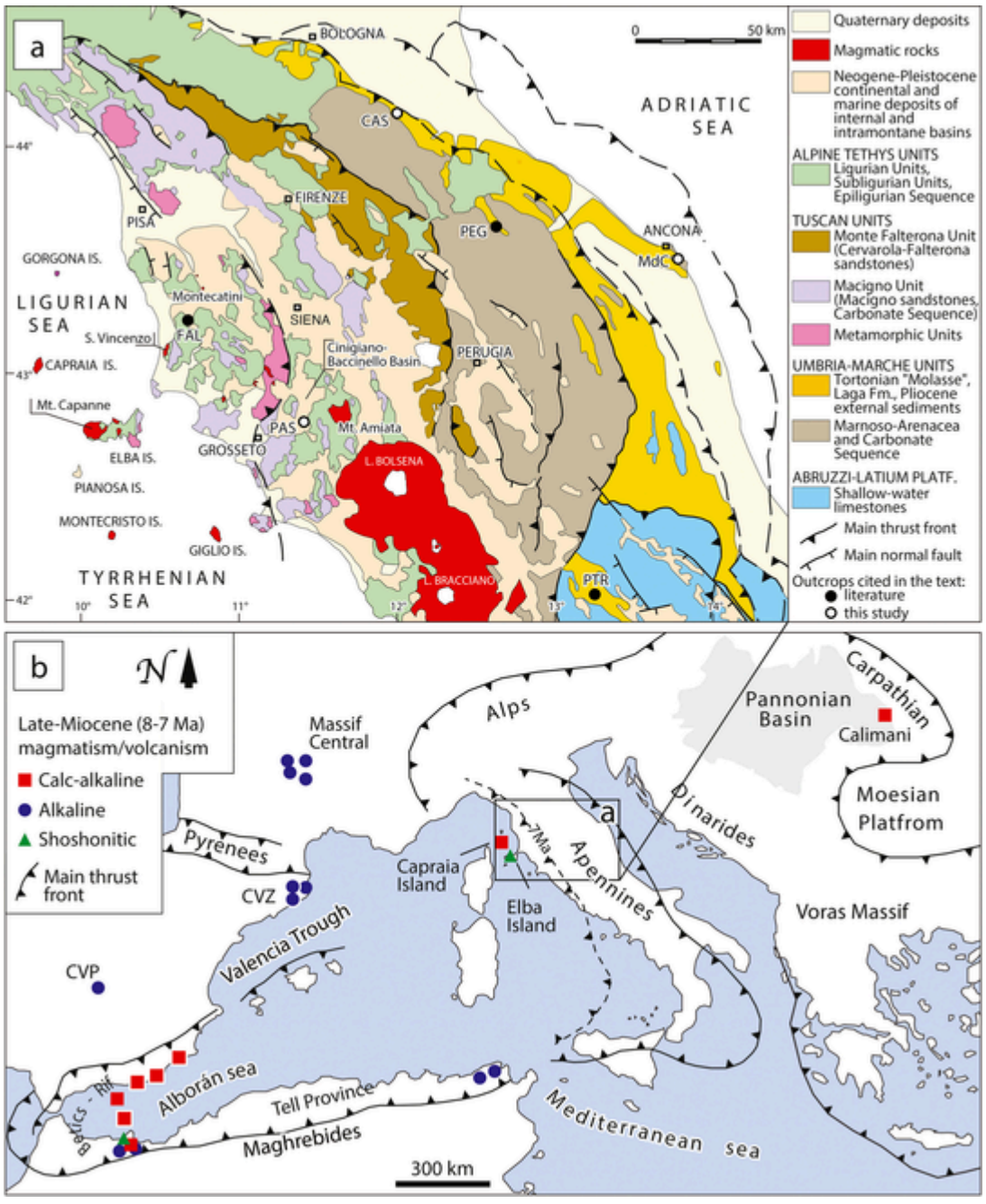

Passonaio layer

The Cinigiano-Baccinello Basin, **AQ5** an Upper Miocene-Pliocene basin in southern Tuscany is one of the largest continental sedimentary basins in the region (Marroni et al. 2015). The basin is an 8-km wide and 18-km long N–S oriented depression. Its Upper Miocene sedimentary infill consists of palustrine, lacustrine, and alluvial sediments up to 500 m thick (Benvenuti et al. 2001). Extensive field surveys carried out in the late 1990s allowed the discovery of a thin tephra layer within a section outcropping at the “Podere Passonaio” site. Rook et al. (2000) analyzed six biotite grains from the Passonaio layer (PAS) by $^{40}Ar/^{39}Ar$ dating, which yielded an average age of 7.55 ± 0.03 Ma.

Faltona layer

The Sassa-Guardistallo Basin is located in western Tuscany, close to the Tyrrhenian Sea. Its sedimentary succession consists of 400-m-thick Upper Miocene continental conglomerates, sandstone, and limestone, overstepping a shaly substratum and overlain by late-Messinian evaporites and marine to continental Pliocene–Pleistocene sediments (Cerrina Feroni et al. 2006). A crystalline tuff layer (FAL) about 5 cm thick, was found at the Faltona quarry interlayered within clay sediments belonging to the Miocene pre-evaporitic

fluvio-lacustrine succession (D'Orazio et al. 1995). The K/Ar dating performed on the biotites yielded an apparent age of 8.07 ± 0.11 Ma. However, this date is to be considered with caution due to low K content of the biotite (D'Orazio et al. 1995).

Pietrasecca layer

The Pietrasecca section (PTR) crops out in the central Apennines. The section is about 60 m thick and is characterized, from the base to the top, by shallow-water limestones, marls, and marly clays, in which the volcanogenic material is embedded. A thick siliciclastic turbiditic succession overlies the section (Cosentino et al. 1997). The volcanogenic material crops out in a few cm-thick, fine-grained yellowish horizon mainly constituted by subeuhedral crystals of plagioclase, quartz, biotite, and K-feldspar (Cipollari et al. 1998). Cosentino et al. (1997) determined an $^{40}Ar/^{39}Ar$ age on plagioclases of 7.17 ± 0.08 Ma (Cosentino et al. 1997).

Peglio horizon

The Peglio section (PEG) is in the internal part of the northern Umbria-Marche Apennines on the south-western flank of a regional NW–SE trending syncline hosting the Pietrarubbia-Peglio Basin. The section is 8 m thick and is characterized by blueish marly clays and silty clays with three interbedded biotite-rich layers and 4–8 cm thick laminated volcaniclastic thin sandstones (Cipollari et al. 1998). The volcanogenic components contain fresh, euhedral crystals of plagioclase, biotite, quartz, and K-feldspar and lava fragments. The analytical results of the biotites dated with the $^{40}Ar/^{39}Ar$ method yielded a plateau age of 7.59 ± 0.07 Ma (Cipollari et al. 1998).

Monte del Casino

The Monte del Casino section (CAS) is situated in the foothills of the northern Apennines (Montanari et al. 2007). The section consists of Upper Tortonian-lower Messinian open marine grey to blue-colored marly clays with numerous intercalations of biotite-rich ash layers and brown to black colored, organic rich, laminated sediments (e.g., Vai et al. 1993). The section contains 19 biotite-rich horizons with few plagioclase and quartz crystals. The biotites are well-preserved and have an idiomorphic shape suggesting a volcanic origin as fallout deposits (Krijgsman et al. 1997; Vai et al. 1993). $^{40}Ar/^{39}Ar$ analyses on biotite crystals yielded two plateau ages of 7.48 ± 0.02 and 7.56 ± 0.07 Ma.

Monte dei Corvi

The Monte dei Corvi section (MdC) is exposed along the coastal cliffs of the Adriatic Sea (Italy). The MdC section encompasses parts of the Serravallian, Tortonian, and Messinian stages (Montanari et al. 2017). It is composed of a cyclic alternation of greenish-grey marls, whitish marly limestones, and brownish sapropels. Several ash layers have been found, and six of them are included in the late Tortonian Rossini Interval (7.62–7.17 Ma). Furthermore, the ash layers in the Rossini Interval have been correlated to those exposed in the Monte del Casino section (Hüsing et al. 2009), and various authors report that the source of the volcanic ashes is still unknown (e.g., Krijgsman et al. 1997; Hüsing et al. 2009). Wotzlaw et al. (2014) sampled the volcanogenic beds in the Rossini interval, and 96 individual zircons were analyzed using high precision U/Pb geochronology.

The Mediterranean volcanism during the late Tortonian

During the late Tortonian, several volcanic centers were active in Spain, Italy, northern Africa (Morocco and Tunisia), central France, and the Carpathian region (Fig. 1 b).

The Massif Central (central-southern France) is the largest magmatic province of the West-European Rift system. This area was marked by a volcanism of variable intensity, whose origin was suggested to be caused by a localized hot spot in the mantle (Michon and Merle 2000). A **AQ6** significant magmatism occurred during the period 9–6 Ma, producing sub-alkaline and alkaline intraplate lavas (Michon and Merle 2000). Morphologically, several main volcanoes and scattered monogenetic cones and maars have been recognized, although not representative of any significant explosive volcanism, the products of which could have reached central Italy. For this reason, and mainly because of the geochemistry of the products, we exclude this area as the source of our ash layers.

Coeval alkaline magmatism also occurs in the Valencia trough and neighboring areas. The Calatrava Volcanic Province (CVP) of central Spain is characterized by intracontinental plate basalts extruded during the Late Miocene to Quaternary (Cebriá and Lopez-Ruiz 1995). The Catalan Volcanic Zone (CVZ) exhibits the greatest concentration of mid-Miocene to recent alkaline volcanism in the Valencia trough (Martí et al. 1992) and comprises about 50 well-preserved monogenetic volcanoes (Oms et al. 2015) of leucite/nepheline basaltic and alkali basaltic composition (Bolós et al. 2015). The CVZ has classically been divided in three different sub-zones: L'Empordà (> 12–8 Ma), La Selva (7.9–1.7 Ma), and La Garrotxa (0.5–0.01 Ma) (Martí et al. 2011). Although the ages match with the age of our material, the eruptive type (mainly monogenetic and fissural) and the geochemistry of the volcanism, as well as for the CVP, bring us to exclude them as possible sources for the ash layers under study.

The Tell province, in northern Tunisia, is also characterized by Upper Miocene (~ 8–5.2 Ma) alkaline magmatism (Lustrino et al. 2011) as well as in the Oranie region in western Algeria, where post-orogenic alkaline basalts occurred (~ 10–7 Ma; Coulon et al. 2002). Their limited areal extent, mode of emplacement (only dykes with no pyroclastic components in Tell and lavas in Oranie), and geochemical composition (mostly alkali basalts), however, make this area not suitable for being the source of our ash layers.

Calc-alkaline magmatism occurred in the western Mediterranean in an area known as Betics-Rif orogen from the northwestern coast of Morocco to the southeastern coast of the Iberia peninsula (Mattei et al. 2014). This orogen comprises the Alborán Volcanic Region and includes igneous rocks from northwestern Africa, the Alborán Sea, and the southeastern Spanish coast. Upper Miocene calc-alkaline magmatism in northern Africa occurs mainly in the Gourougou volcanic center in northern Morocco (Lustrino et al. 2011) although it is slightly younger (6.69–4.82 Ma; Duggen et al. 2008) than the ages of our interest. In southeastern Spain, widespread calc-alkaline volcanism is well represented in Cabo de Gata (~ 14.4–6.6 Ma), Vera (~ 7.5–6.4 Ma), Mazarron (~ 8.9–6.8 Ma), and Murcia (~ 8.1–6.8 Ma) areas (Duggen et al. 2008). This volcanism is characterized by explosive eruptions leading to the formation and deposition of pyroclastic and effusive products that erupted from submarine vents and deposited in submarine settings (Mattei et al. 2014). The geochemistry of the

products could be compatible with the volcanism that erupted the ash layers in central Italy, but the fact that this volcanism is subaqueous represents the main limitation to consider this area as the possible source of our layers, which were emplaced from a sub-aerial activity.

In eastern Europe, and specifically in the Carpathian orogen, Miocene-Quaternary magmatism developed in different stages from 20 to < 0.1 Ma (Pécskay et al. 1995) and consisted of large volumes of calc-alkaline magmatic products, ranging from basalts to rhyolites. The late Miocene expression of the magmatism that characterized the region is in the Calimani mountains, in the eastern Carpathians volcanic arc, where calc-alkaline acidic and intermediate volcanic activity occurred from 11.3 to 6.7 Ma (Seghedi et al. 2005). According to Seghedi et al. (2005), late Tortonian (8–7 Ma) activity is mainly characterized by the extrusion of andesitic-dacitic lava domes and basaltic to andesitic lava flows, while pyroclastic products are much less common and with limited dispersion. The mainly effusive nature of the erupted products, the limited amount of pyroclasts, and the west-to-east predominant winds (Quan et al. 2014) during that period suggest that this region is also not the one from which our ash layers might come from.

Upper Miocene Tyrrhenian magmatism

Another region that was characterized by active volcanism during the late Tortonian is the Tuscan Magmatic Province (TMP) in the Tyrrhenian region of Italy. This region, located at the tectonic boundary between the converging Africa and Europe plates, is the youngest deep basin in the Mediterranean Sea. During the late Miocene, the classical model proposes that magmatic activity initiated in concomitance with a significant change from a compressional to an extensional geodynamic regime (Savelli 1988). Ma **AQ7** gmatism started in the northern Tyrrhenian region, in an ensialic back-arc extensional setting and gave rise to the igneous products of the TMP ranging in age from about 14 Ma at Sisco (Corsica) to about 0.3 Ma at the Monte Amiata (Tuscany). The igneous activity formed acidic peraluminous intrusive bodies and the eruption of rhyolites, as well as calc-alkaline and shoshonitic lavas and hypabyssal bodies. Pyroclastic rocks in the TMP are scarce occurring as ignimbrites around Monti Cimini and Cerite (3.5–0.9 Ma) (Poli et al. 2003) as well as minor pyroclastic deposits in the easternmost flank of the Capraia island. The ash layers under investigation were deposited between the Tortonian and the Messinian with ages between 8 and 7 Ma. In this timeframe, andesites and rhyo-dacites of high-K affinity erupted on the Capraia island. The latter is a ~ 20 km^2 stratovolcano in the northern Tyrrhenian Sea, (Fig. 1a) that was built during two different periods of activity. This is the only known active volcanic center developed during the period 8–7 Ma in the peri-Tryrrhenian area. The first build-up period occurred between 7.8 and 7.1 Ma according to available geochronological data (Santo 2021). Aldighieri et al. (1998) dated biotite crystals from lavas using K/Ar methods yielding a range of ages from 7.59 ± 0.07 Ma to 7.25 ± 0.06, whereas Gasparon et al. (2009) used $^{40}Ar/^{39}Ar$ analyses on biotites, plagioclases, and whole rock showing similar results (7.75 ± 0.09 Ma to 7.16 ± 0.31). More recently, Gagnevin et al. (2011) obtained a weighted mean $^{206}Pb/^{238}U$ age of 7.29 ± 0.05 Ma using zircons from one dacite. At the same time, another magmatic center in the TMP was also active, namely the Elba Island central-western magmatic complex (Dini et al. 2002). The igneous sequence started with the construction of a multilayer laccolith complex, successively intruded, and deformed by the emplacement of the monzogranitic Monte Capanne pluton and its associated leucocratic dikes (Farina et al. 2010). Finally, a swarm of more mafic dikes were emplaced, cutting through the entire succession.

Methods

Samples

The analyzed samples are from three different localities in northern-central Italy (Fig. 1a): the Passonaio (PAS—one layer), Monte dei Corvi (MdC—two layers), and Monte del Casino section (CAS —two layers) sections. PAS is an altered 1-cm-thick orange layer embedded in the upper Neogene Baccinello-Cinigiano lacustrine sequence (Fig. 2a). The layer is biotite-rich and contains altered plagioclase crystals, rare quartz, devitrified glass, and zircons. In contrast, the MdC and CAS layers are compacted greyish marly limestones in which abundant biotite crystals are embedded (Fig. 2b, c). In order to verify if the samples are derived from the same volcanic source, we have separated out the biotite crystals for geochemical comparison. For MdC and CAS, we analyzed the two oldest layers (MdC1, MdC2 and CAS1, CAS2).

Fig. 2

Details of the outcrops of the tephra layers in the three selected locations studied in the present work. **a** PAS, Passonaio outcrop, southern Tuscany. **b** MdC, Monte dei Corvi beach outcrop on the central-eastern coast of Italy, here are present both MdC1 and MdC2 layers. **c** CAS–Monte del Casino outcrop, eastern side of northern Apennines, in the photograph is represented only one (CAS1) of the two layers analyzed

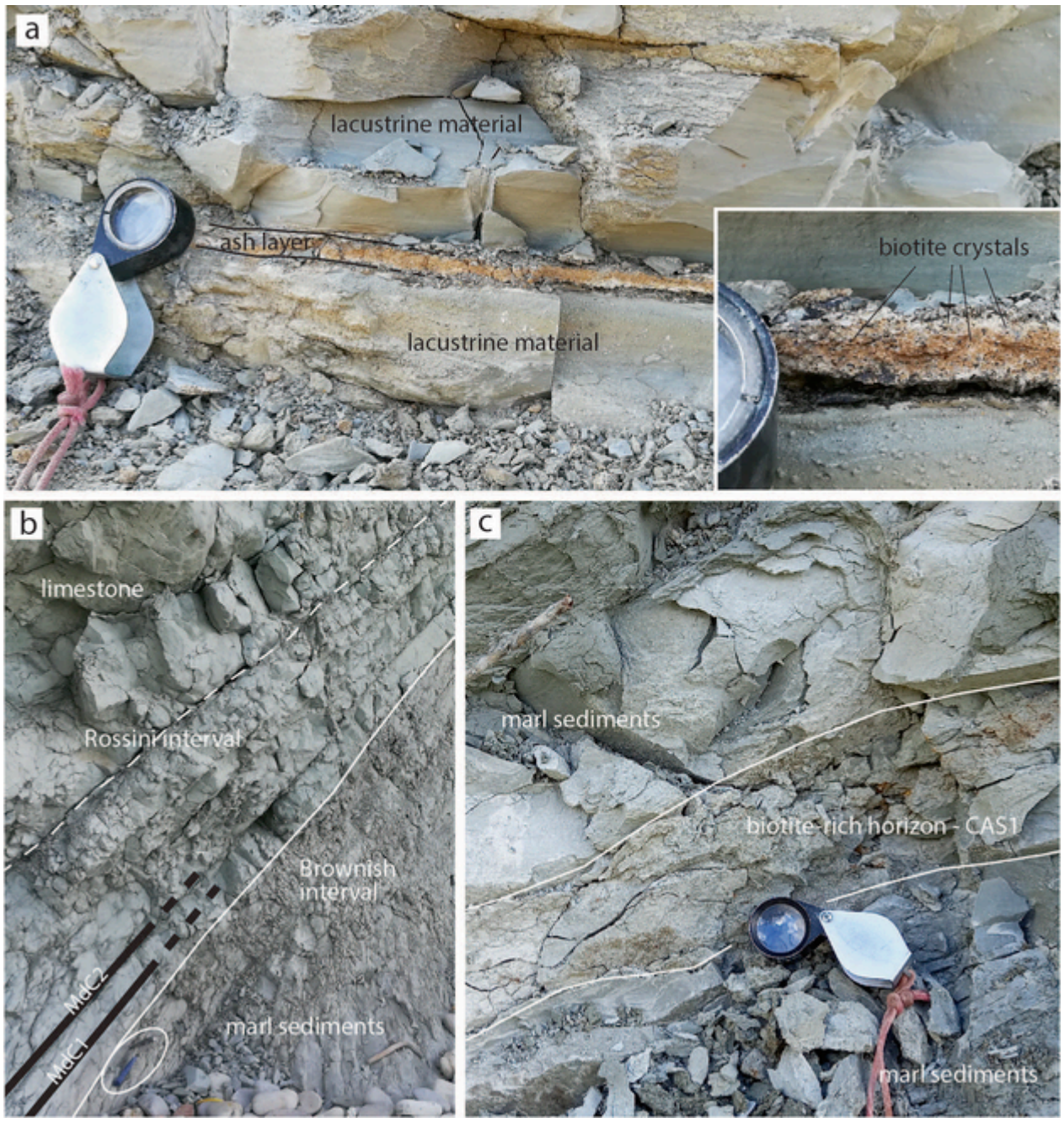

To determine the possible geographic source location(s) of the eruptive center(s), we also analyzed biotite crystals from different localities and lithologies of Capraia island (Fig. 3), preparing thin-sections of the lavas (CAP1, CAP7, CAP~~Θ~~31, CAP35 = L-CAP) and pyroclasts (P-CAP) samples. These data are compared with a dataset of chemical composition from other analyses from the TMP such as the Monte Capanne (MCP) at Elba Island (Farina 2008).

Fig. 3

a Satellite image of Capraia island with the location of the samples collected for the present research. **b** Succession of pyroclastic material cropping out along the eastern coast of the island. **c** Detailed of a pumice clast (CAP4) sampled for geochemical and geochronological analyses

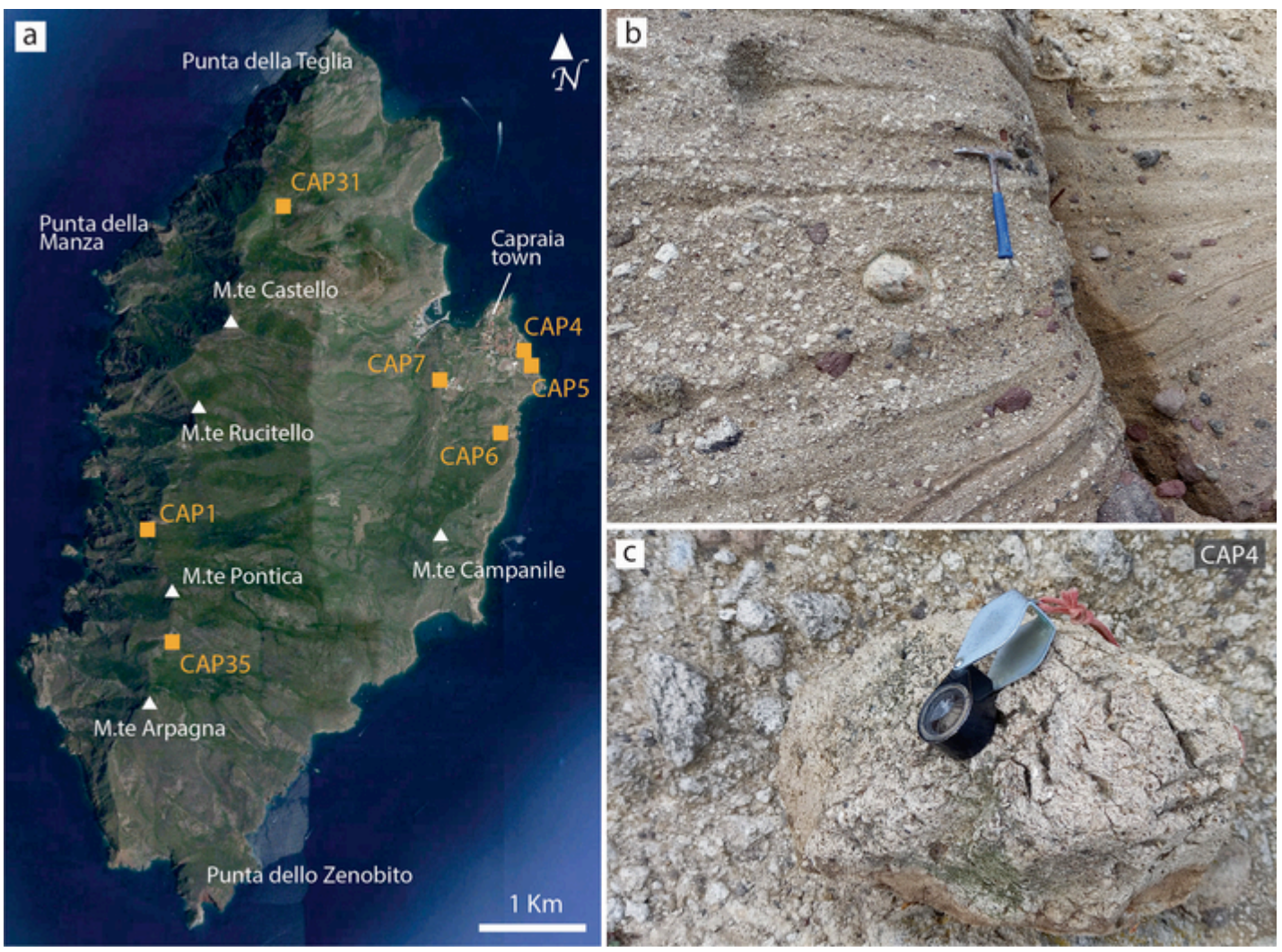

Zircon crystals were separated from the PAS ash layer and three samples of pyroclastic deposits in Capraia (CAP4, CAP5, CAP6 = P-CAP). To avoid misunderstandings, it is worth mentioning that we decided not to analyze zircons from MdC because detailed analyses

have already been conducted by Wotzlaw et al. (2014) using the same technique and in the same lab, and as for CAS, because no zircons have been found at that locality. The separation procedure was conducted at the University of Geneva (Switzerland) and involved standard rock crushing and density and magnetic separation. For PAS ID-TIMS dating, we used seven zircons. For other analyses, ca. 200 zircon crystals were handpicked and mounted in epoxy resin blocks from each sample. The mounts were polished to expose the crystal interior and imaged by cathodoluminescence using a JEOL JSM-7001F Schottky scanning electron microscope available at the University of Geneva. Cathodoluminescence images and texture descriptions are included in the supplementary material (Fig. SM1).

Electron microprobe analysis

In situ mineral analyses of biotite were performed using a JEOL 8200 Superprobe at the University of Geneva. The microprobe is equipped with a five-channel wavelength dispersive spectroscope system (WDS) and was operated at an accelerating voltage of 15 keV, a beam current of 15 nA, and a beam diameter of 5 µm. Quantitative analyses were made using a variety of internal standards (orthoclase [Si,K], andalusite [Al], albite [Na], forsterite [Mg], fayalite [Fe], wollastonite [Ca], Mn-Ti oxide [Mn,Ti], and Cr oxide [Cr]). The biotite formula has been calculated following Li et al. (2020).

U–Pb geochronology (ID-TIMS)

For chemical abrasion ID-TIMS (CA-ID-TIMS) analysis, zircons were first annealed at 950 °C for 48 h, and then, to minimize the effects of secondary lead loss, each zircon grain was chemically abraded in HF + trace HNO_3 at 210 °C for 12 h.

Each single zircon fragment was loaded for dissolution into Savillex capsules, spiked with 8–14 mg of the EARTHTIME ^{202}Pb-^{205}Pb-^{233}U-^{235}U tracer solution (Condon et al. 2015) and dissolved in 70 µl HF and traces of HNO_3 at 210 °C for about 60 h in Parr bombs. After evaporation the residue was re-dissolved in HCl. Lead and uranium from zircons were separated by anion exchange chromatography (Krogh 1973) in 40 µl columns using ultra-pure HCl and H_2O, and finally dried down with 3 µl of 0.02N H_3PO_4.

The isotopic analyses were performed on a TRITON mass spectrometer equipped with a MasCom electron multiplier (SEM). Lead and uranium isotopic fractionation was corrected online using the $^{202}Pb/^{205}Pb$ and ^{233}U-^{235}U ratio of the tracer. Lead and uranium (as UO_2) isotope compositions were measured on the electron multiplier and Faraday mode respectively. Isobaric interference of $^{233}U^{18}O^{16}O$ on $^{235}U^{16}O^{16}O$ was corrected using a $^{18}O/^{16}O$ ratio of 0.00205. The measured uranium isotopic ratios were corrected assuming a sample $^{238}U/^{235}U$ ratio of 137.818 ± 0.045 (2σ, Hiess et al. 2012). All common Pb in the zircon analyses were attributed to the procedural blank. Data reduction was done using the TRIPOLI and Redux software (Bowring et al. 2011). All $^{206}Pb/^{238}U$ and $^{207}Pb/^{206}Pb$ ratios were corrected for initial disequilibrium in $^{230}Th/^{238}U$ using a partition coefficient ratio D_{Th}/D_U of 0.2 ± 0.1 (2σ). The uncertainty about the disequilibrium correction is also propagated into the uncertainty of $^{206}Pb/^{238}U$ dates.

U–Pb geochronology (LA-ICP-MS)

Zircon U–Pb dating was carried out by laser-ablation inductively coupled plasma mass spectrometry (LA-ICP-MS) at the Department of Earth Sciences of the University of Milano. The analyses were performed using a Thermo Fisher Scientific iCAP RQ ICP-MS coupled to a 193-nm excimer laser ablation system (Analyte Excite by Teledyne Photon Machine). The analyses were carried out with a laser spot of 25 µm, a laser fluence of 3.0 J/cm^2, and a repetition rate of 7 Hz. Data were acquired using a routine where 35 s of background measurement was followed by 60 s of ablation. The integration time used was 10 ms for all the masses analyzed (^{238}U, ^{232}Th, ^{208}Pb, ^{207}Pb, ^{206}Pb, ^{204}(Pb + Hg), and ^{202}Hg. Laser-induced elemental fractionation and instrumental mass fractionation were corrected by normalization to reference zircon Plešovice (Sláma et al. 2008). To test the accuracy and external reproducibility of the obtained age data, multiple analyses of zircon crystal 91,500 (Wiedenbeck et al. 1995) were performed. Among these, 30 zircons yielded a $^{206}Pb/^{238}U$ age of 1060.4 ± 3.7 (MSWD = 1). The calculated age is identical within yielded uncertainty to the value reported by Wiedenbeck et al. (1995). Data reduction was carried out using the Glitter software (Griffin et al. 2008). Concordia age and weighted mean calculations were performed with IsoplotR (Vermeesch 2018).

Trace element analysis of zircon crystals

Zircons were analyzed for trace elements by LA-ICP-MS. We used a Thermo Scientific ICP-MS iCAP RQ single quadrupole interfaced to a 193-nm ArF excimer laser ablation system housed at the Department of Earth Sciences of the University of Milan. Before the analytical session, the instrument was tuned in linear scan mode on NIST-SRM 612 silicate glass, and oxide generation was mitigated by keeping the$^{140}CeO^+/^{140}Ce^+$ (with O referring to ^{16}O) < 0.3. In order to correct for the instrumental drift, NIST-SRM 612 was measured twice after every ten zircon analyses. The spot analyses were performed using a 10-Hz repetition rate and a laser output energy of 2 J/cm^2 with an ablation spot size of 25 µm. Each analysis consisted of 40-s background measurement followed by 60 s of laser ablation. Dwell times were 5 ms for ^{29}Si and ^{90}Zr, 100 ms for ^{49}Ti, and 30 ms for all the other analytes. For concentration calculations, average background-subtracted count rates were internally normalized to ^{29}Si using the stoichiometric SiO_2 wt% content in zircon (i.e., 32.78 wt%). The glass BCR-2 was used as secondary standard. The raw data were processed using the GLITTER software package (van Achterbergh et al. 1999).

Zircon Lu–Hf isotope analysis

Lu and Hf isotopic ratios were determined at the University of Ouro Preto (Brazil) using a Thermo-Fisher Neptune MC-ICPMS coupled to a Photon Machines 193 (λ = 193 nm) ArF excimer laser ablation system. The 50-mm spot-size laser was fired at 5-Hz repetition rate and 3 J*cm^{-2} energy density. Corrections for background signal, instrumental mass bias, and isobaric interferences of Lu and Yb isotopes on mass 176 were done following Gerdes and Zeh (2009). Quoted uncertainties are quadratic additions of the within-run precision and the reproducibility of the reference zircons Temora (Wu et al. 2006), 91,500 (Blichert-Toft 2008), Mud Tank (Woodhead and Hergt 2005), and BB (Santos et al. 2017). Five reference materials were used during the runs: Mud Tank, Temora, GJ-1, 91,500, and BB. Analyses of the reference zircon agree within error with their recommended values. Initial $^{176}Hf/^{177}Hf$ ratios were calculated from the measured

$^{176}Lu/^{177}Hf$ and $^{176}Hf/^{177}Hf$ ratios using a ^{176}Lu decay constant of $\lambda = 1.867 \times 10^{-11}$ a^{-1}. Epsilon Hf values were calculated using Chondritic Uniform Reservoir (CHUR) $^{176}Lu/^{177}Hf$ and $^{176}Hf/^{177}Hf$ ratios of 0.0336 and 0.282785, respectively.

Results

Mineral chemistry—biotite

The composition of biotite crystals from five ash layers (PAS, MdC1, MdC2, CAS1, CAS2) (Table 1_SM in supplementary material) is compared with the composition of biotites from other igneous rocks of the TMP of similar age and are shown in Fig. 4. These are (1) lavas and pyroclastic deposits from Capraia (L-CAP and P-CAP) and (2) Monte Capanne pluton and Cotoncello dike from Elba Island (Farina 2008). In Fig. 4 a, we plot the mole fraction of the annite component in biotite (X_{Bt} Annite; the fraction of Fe_{2+} in the octahedral site) vs. Al_{tot} (apfu, atoms per formula unit). Biotites from the ash layers form a positive linear array and limited, but significant compositional differences are observed. Biotite from PAS has the lower Al_{tot} and annite fraction, with Al_{tot} between 1.2 and 1.3 apfu and X_{Bt} Annite between 0.250 and 0.300. Biotites of the two samples from MdC have identical composition and exhibit limited scatter (average $Al_{tot} = 1.299$, $\sigma = 0.022$), partially overlapping with the composition of biotite from PAS. The two samples from CAS are enriched in Al_{tot} and annite and show a larger compositional scatter; CAS2 has an average Al_{tot} of 1.353 ($\sigma = 0.028$) and CAS1 of 1.415 ($\sigma = 0.028$).

Table 1

U–Pb isotopic data for zircons from PAS AQ8 ash layer at Passonaio locality in southern Tuscany

Fraction	Dates (Ma)						Composition			
	$^{206}Pb/^{238}U^{a}$	±2σ abs	$^{206}Pb/^{238}U^{b}$	±2σ abs	$^{207}Pb/^{235}U^{b}$	±2σ abs	Th/U[d]	Pb* (pg)[e]	Pb_c (pg)[f]	Pb*/ Pb_c[g]
Pas										
z1f	7.565	0.015	7.474	0.012	7.66	0.14	0.7	2.74	0.49	5.593831
z2f	7.563	0.010	7.4727	0.0073	7.595	0.072	0.9	2.69	0.19	14.042656
z3f	7.574	0.016	7.484	0.012	7.71	0.14	0.6	1.05	0.15	6.795519
z6f	7.593	0.026	7.503	0.024	7.76	0.28	0.6	0.653	0.26	2.545927
z7	7.561	0.033	7.470	0.032	7.59	0.40	0.7	0.629	0.33	1.877210
z8	7.577	0.060	7.486	0.060	7.61	0.64	0.7	0.398	0.34	1.167081
z9	7.561	0.016	7.471	0.013	7.56	0.15	0.7	1.72	0.35	4.938659

	Isotopic Ratios					
	$^{206}Pb/^{204}Pb^{h}$	$^{207}Pb/^{235}U^{i}$	±2σ %	$^{206}Pb/^{238}U^{i}$	±2σ %	Corr. coef
Pas						
z1f	327	0.00757	1.8	0.0011601	0.16	0.752
z2f	757	0.007508	0.96	0.0011599	0.098	0.721
z3f	397	0.00762	1.8	0.0011616	0.16	0.849
z6f	159	0.00767	3.6	0.0011646	0.32	0.751
z7	123	0.00750	5.2	0.0011594	0.43	0.763
z8	82	0.00752	8.4	0.0011619	0.80	0.683
z9	291	0.00748	2.0	0.0011596	0.17	0.749

Fig. 4

Chemical composition of biotites. **a** Mole fraction of the annite component in biotite (XBt Annite; fraction of Fe2 + in the octahedral site) vs the total aluminum (apfu). **b** K (apfu) vs the total aluminum (apfu). **c** Fe# vs total aluminum (apfu)

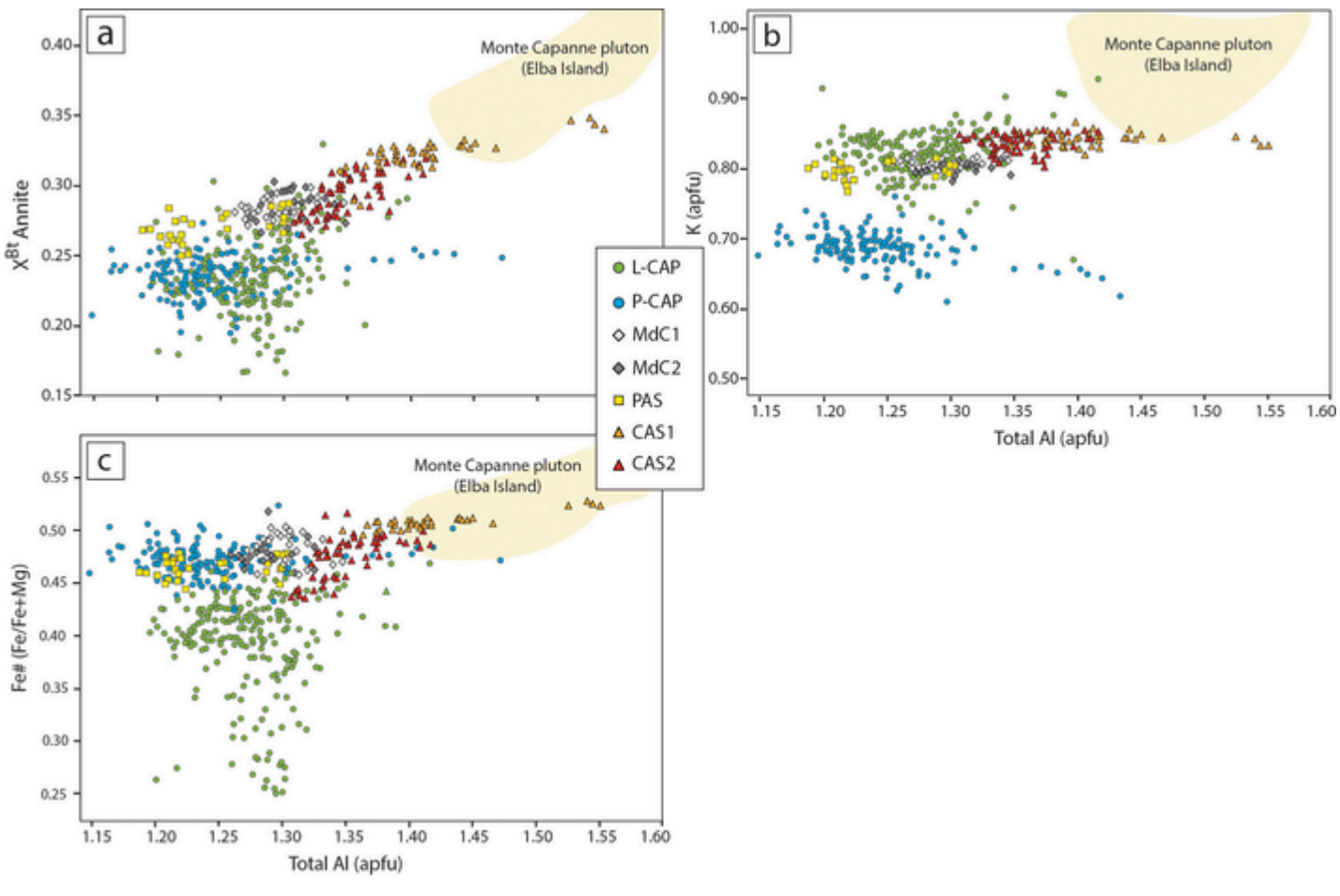

Biotites from Capraia island show Al_{tot} content similar to that of biotites from PAS and MdC, while those from the CAS ash layers have higher Al content. However, biotites from Capraia island have a lower annite component than the biotites characterizing the different ash layers. Finally, biotite from the western intrusive complex of Elba island (i.e., Monte Capanne pluton and Cotoncello dike) are strongly enriched in Al and Fe^{2+}.

By plotting the data in a Al_{tot} vs. K (apfu) diagram (Fig. 4 b), we observe that the biotites from the pyroclastic deposits of Capraia island have low K (ca. 0.7 apfu) with respect to the composition of biotites from the other units. The low K of these biotites is associated with total oxides contents between 85 and 93 wt%, indicating alteration of the biotite to chlorite with loss of K from the interlayer site (Eggleton and Banfield 1985). Th **AQ9** e Fe# (Fe/(Fe + Mg) of biotites from the ash layers and from the pyroclastic deposits of Capraia island overlaps (Fe# = 0.47), while the biotites from the Elba Island are enriched in Fe (Fe# = 0.52; (Fig. 4 c). The Fe# of biotites from Capraia lavas is highly variable ranging from 0.25 to 0.45, but overall these biotites are more magnesium rich, with a cluster of Fe# at ca. 0.40.

Zircons geochronology

U–Pb ID-TIMS analysis on PAS zircon grains is reported in Table 1 with internal errors only, including counting statistics, uncertainties in correcting for mass discrimination, and the uncertainty in the common (blank) Pb composition. The MSWD values of weighted mean $^{206}Pb/^{238}U$ dates are out of range, while for $^{207}Pb/^{206}Pb$ dates are in the range of acceptable values at 95% confidence level and for n^{-1} degrees of freedom, defined by Wendt & Carl (1991).

All seven analyses of individual zircon crystals are concordant within analytical uncertainty and yielded weighted mean $^{206}Pb/^{238}U$ date of 7.5667 ± 0.0064/0.0068/0.011 Ma (n = 7, MSWD = 1), which is interpreted as the best estimate for the age of the volcanic ash (Fig. 5). This age is in agreement with a ^{40}Ar-^{39}Ar of 7.55 ± 0.03 determined by Rooks et al. (2000) on biotites from the PAS layer.

Fig. 5

Concordia age of seven zircons using U–Pb ID-TIMS technique from PAS layer

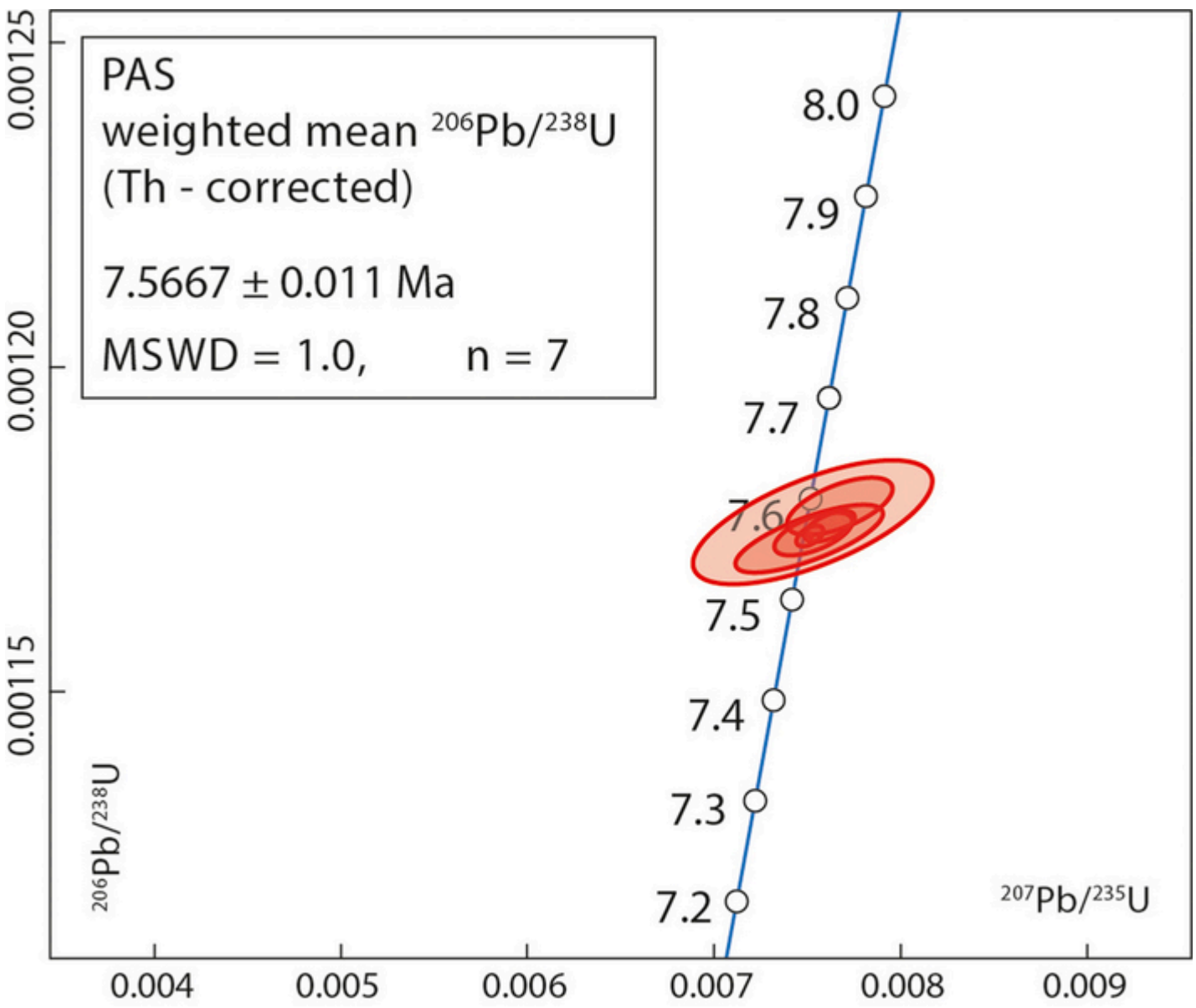

Sixty-seven zircon grains were dated by laser ablation ICP-MS (Fig. 2_SM and Table 2_SM in supplementary material) from three samples of pyroclastic deposits (P-CAP) from the Capraia island. Most of the spot analyses are concordant to sub-concordant, and only those that passed the < 20% discordancy test were considered (i.e., 56 analyses in total). These analyses were mostly performed on zircon rims and gave $^{206}Pb/^{238}U$ spot ages ranging from 7.41 to 6.83 Ma. Zircons from sample CAP4 gave a $^{206}Pb/^{238}U$ weighted mean of 6.97 ± 0.05 Ma with a MSWD of 1.4. This age is identical to the weighted mean age obtained from zircons from CAP6 (7.044 ± 0.091 Ma, MSWD = 2.4) and CAP5 (6.886 ± 0.093 Ma, MSWD = 2.0). No inherited cores were observed in catholuminescence or analyzed.

Zircon trace element composition

The composition of zircon from the different samples of Capraia pyroclastic rocks overlaps, and thus these are described together and compared with the composition of zircons separated from the PAS ash layer. Zircon crystals collected from the PAS ash layer are different with respect to those sampled from the Capraia pyroclastic rocks (P-CAP) (Fig. 6). PAS zircons have U content ranging between 266 and 808 ppm (average = 495 ppm) and Th between 106 and 531 (average = 290 ppm), while zircons from Capraia island have higher Th and U

contents, showing average values of 625 and 1575, respectively. For both dataset, good positive linear correlations between Th and U can be observed, but Th/U is higher in PAS sample (0.57) than in Capraia island (0.39). The average Ti content for PAS zircons is 11.6 ppm (1SD = 2.9) and the average Eu/Eu* (i.e., Eu√(Sm*Gd)) is 0.07. These values are higher than values observed for the zircon in Capraia pyroclastic rocks, having a Ti content of 3.1 (1SD = 1.3) and Eu/Eu* of 0.05. Less pronounced compositional differences are also observed in Hf, HREE, Y, and Yb/Dy, which are higher in the zircons from Capraia island than in PAS. No correlations are observed for U vs Eu/Eu, Yb/Dy, or Hf for both Capraia and PAS zircons.

Fig. 6

Zircon trace elements composition from the different samples of Capraia island pyroclastic rocks (P-CAP = CAP4, CAP5, CAP6) compared with the composition of the zircons separated from the PAS ash layer

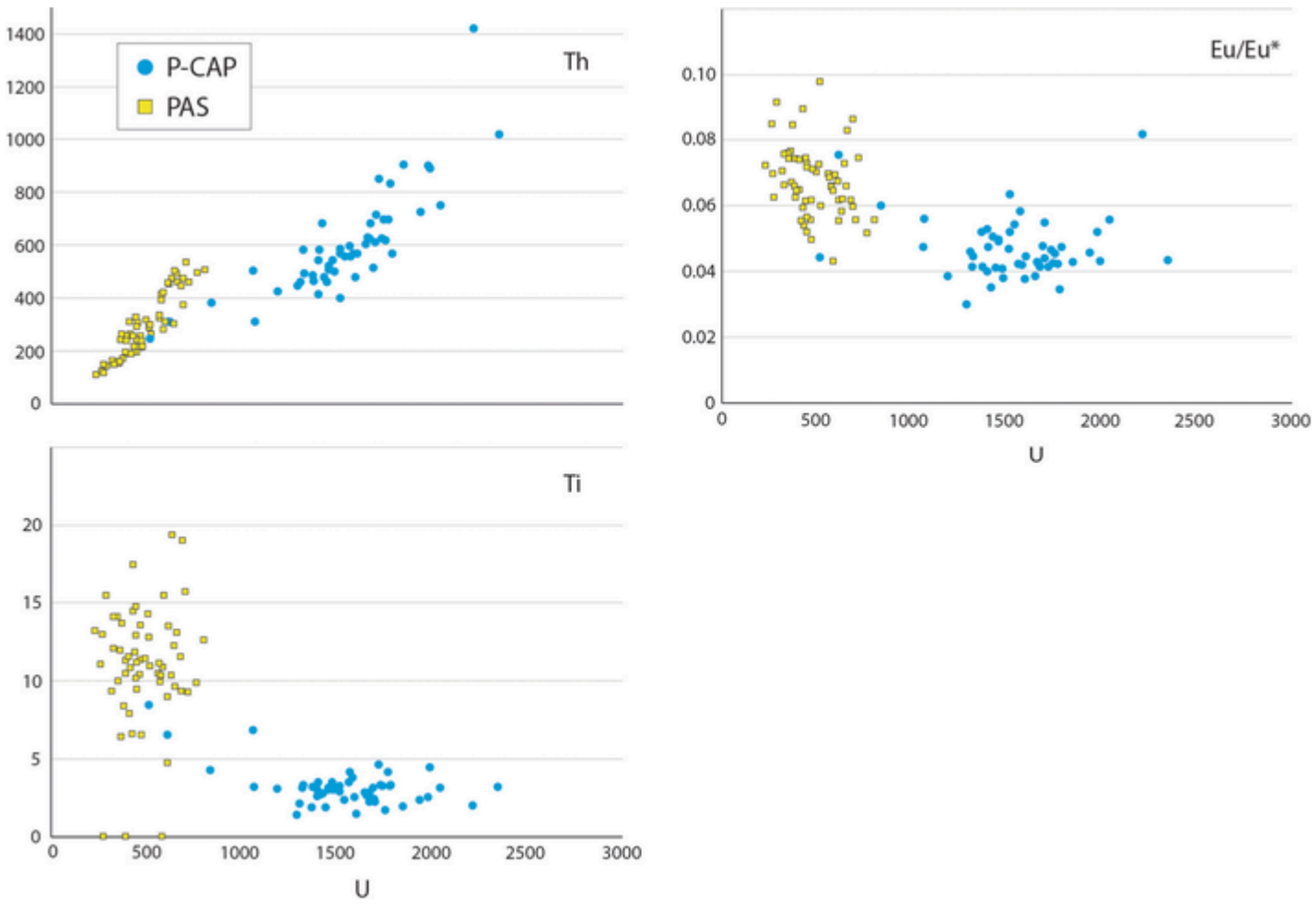

Zircon Hf isotopic composition

Zircon crystals from Capraia island and the PAS ash layer show a distinct crustal hafnium isotope signature, with ε_{Hf} values ranging between − 4.1 and − 7.3 (Fig. 7). Zircon grains from individual samples exhibit a modest isotopic variability of 3.2 epsilon units. Although, this range is between two and six times larger than the 2σ uncertainty determined on individual spot analyses, ca. 90% of data fall in a more restricted range of 2 epsilon units. Importantly, the extreme ε_{Hf} values do not appear to be correlated to specific textural domains. Zircons from Capraia island have very similar average ε_{Hf} values of − 5.1, − 5.5, and − 5.6 for samples CAP4, CAP5, and CAP6 (P-CAP), respectively. Taking into consideration the standard deviation, which varies between 0.52 and 0.65 (1σ) depending on the sample, the Hf isotopic composition of the three samples is identical. Zircon grains from PAS sample have an average ε_{Hf} value of − 5.9 and a standard deviation of 0.77. Thus, their isotopic signature overlaps with the composition of zircon from Capraia island.

Fig. 7

Hf isotope composition of zircon crystals from the Tuscan Magmatic Province. **a** Spot analyses on zircon crystals from Capraia island (CAP4/5/6) and the PAS ash layer. The vertical error bar indicates the 2σ uncertainty on individual analysis. Horizontal dark grey lines represent the average calculated for the different samples. The light grey fields are the standard deviations. **b** Box and whiskers plot for the Monte Capanne pluton, Capraia dacitic lavas, and San Martino porphyry (Gagnevin et al. 2011) and the Plio-Pleistocene granitoids from Tuscany (Farina et al., 2018)

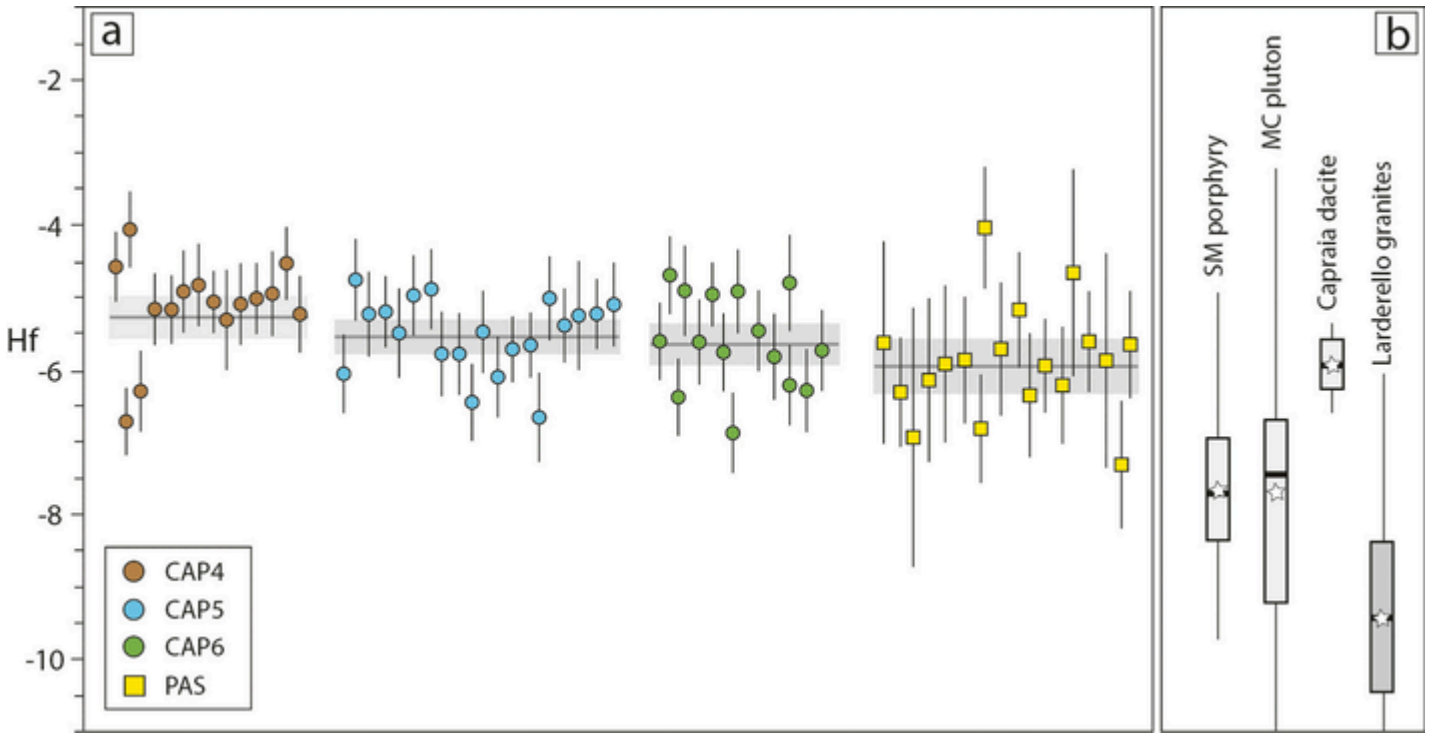

Discussion

In the Tortonian and Messinian, between 11.6 and 5.3 Ma, the retreat of the Adria subducting plate led to the emplacement and eruption of felsic magmas in the Tyrrhenian Sea and to the deposition of ash layers. In this period, and specifically during the span from 8 to 7 Ma, the only active centers known were the Elba island (shallow-level plutonic rocks) and the Capraia island (subaerial volcanism).

The age of the ash layers is coeval with the magmatic activity of western Elba as well as with the eruption of dacitic lavas on the Capraia island. Before using the available data to explore in detail the possible correlation between the distal ash layers and their sources, it is worth discussing the interpretation of U–Pb and Ar–Ar dates in magmatic systems. Most of the data presented in Fig. 78 are $^{206}Pb/^{238}U$ zircon dates obtained by CA-ID-TIMS, a technique that allows reaching an unparalleled precision for single zircon $^{206}Pb/^{238}U$ dates (Szymanowski and Schoene 2020). For instance, today zircon U–Pb dating by CA-ID-TIMS may be better than 0.1% (2σ)—which is equivalent to ca. 7 kyr for zircon crystallized in the Tortonian. Such high precision has led to the recognition that in many igneous rocks, zircon records a prolonged history of crystallization providing insights into the duration and rates of magma reservoir processes (Farina et al. 2024). However, the common occurrence of U–Pb age scatters in populations of zircon crystals from individual samples are critical when we use this mineral to date ash layers, as zircon crystallization can significantly pre-date eruption. This is consistent with $^{40}Ar/^{39}Ar$ ages obtained on sanidine and biotite from silicic volcanic rocks, which are generally younger than U–Pb zircon ages. Although exceptions are described in the literature, this is due to the lower closure temperature of Ar in high-K minerals (< 550 °C). In Fig. 8, we have compared the age obtained from PAS (present work), MdC1 and MdC2 (Wotzlaw et al. 2014), and CAS (Krijgsman et al. 1997) with the age of the Monte Capanne pluton and San Martino porphyry at Elba island and with lavas (Gagnavin et al. 2011) and pyroclastic deposits at Capraia island (P-CAP, present work). The five ash layers considered likely represent four distinct eruptions. Zircon crystals from MdC1 and MdC2 have the same age within error and identical biotite composition, but they come from two distinct ash beds, which are located less than half a meter above the other in the same stratigraphic sequence. Zircons from PAS have a weighted age almost identical to the weighted age of MdC2, with the two ages that do not overlap for only 1 ka. However, the two layers have identical biotite composition.

Fig. 8

Geochronology of Tortonian ash layers and igneous rocks of the Tuscan Magmatic Province. The diagram combines zircon ^{238}U-^{206}Pb (bars) as well as biotite and plagioclase ^{40}Ar-^{39}Ar data (squares). U–Pb original data of the present work are in orange bars both for LA-ICP-MS (Capraia; P-CAP) and ID-TIMS (PAS) techniques; while from Wotzlaw et al. 2014 (MdC1 and 2—white bars), Barboni et al., 2015 (Elba island—light blues bars), and Gagnevin et al. 2011 (lavas from Capraia island—grey bar). ^{40}Ar-^{39}Ar data are from Krijgsman et al. 1997 (CAS); Gasparon et al. 2009 (Capraia)

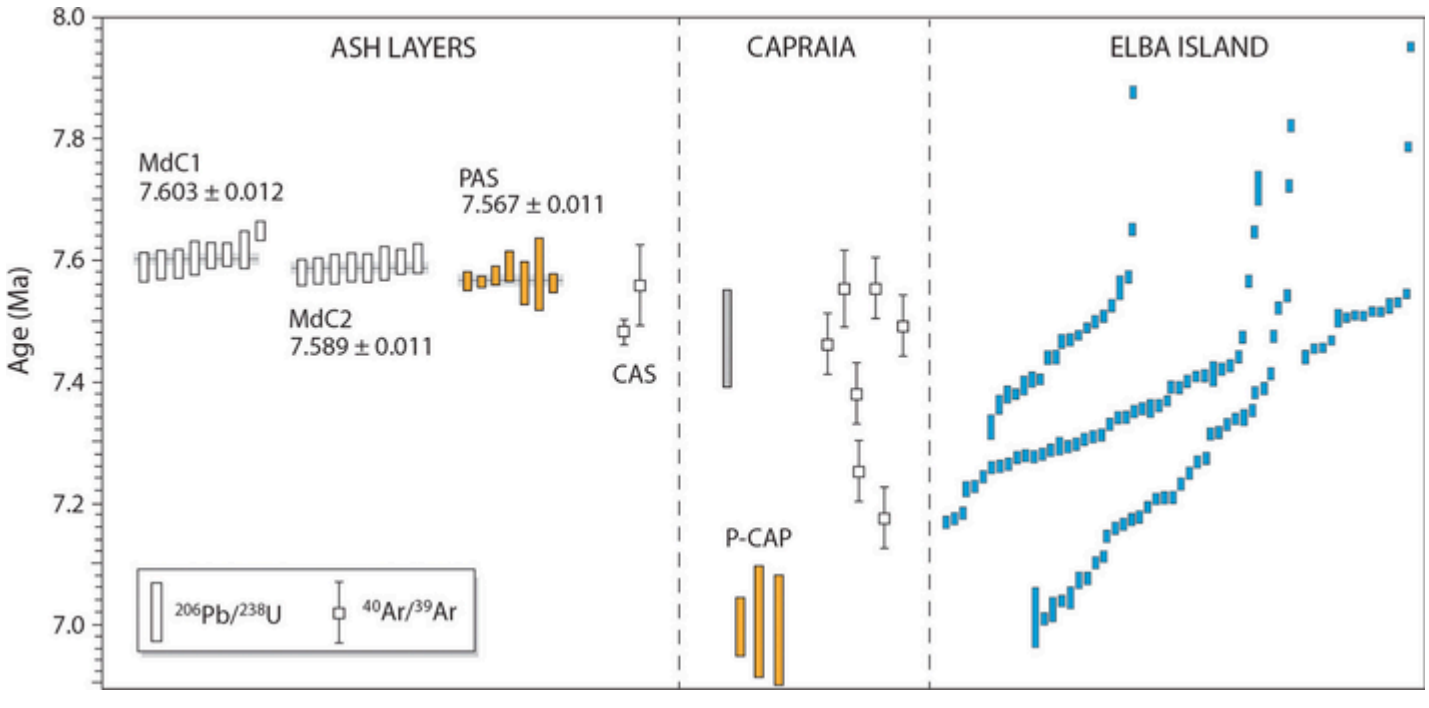

The $^{40}Ar/^{39}Ar$ biotite ages for CAS yield two results, the oldest plateau age has a significant uncertainty although some authors report that the experiment allows the calculation of an age that meets commonly accepted criteria. This age matches with the PAS sample as shown in

Fig. 8. The second biotite plateau age for CAS sample yielded 7.48 ± 0.02 Ma, a value that is 80–120 kyrs younger than the age of previous layers. Moreover, the composition of biotites in CAS is significantly different from the composition of biotites in PAS and MdC, indicating that the former was deposited during a different volcanic event.

The first zircon crystals in the Monte Capanne pluton started crystallizing at ca. 8 Ma, which is also the age of the oldest intrusive units of the island (Farina et al. 2010). However, the youngest zircons in the three units forming the pluton crystallize at ca. 7.3, 7.2, and 7.0 Ma. Therefore, although the magmatic system was already active during the deposition of the central Italian ash layers, the final emplacement of the pluton postdates by 200–500 kyrs the age of the zircons in the ash layers under investigation. Most of the zircon in the San Martino porphyry crystallize between 7.541 ± 0.006 and 7.437 ± 0.011 Ma and are therefore only 10–60 kyrs younger than zircons from the ash beds.

Zircon crystals extracted from a dacitic lava on the Capraia island yielded a $^{206}Pb/^{238}U$ age of 7.458 ± 0.077 Ma (recalculated from the data reported in Gagnevin et al. 2011). However, this is a relatively poorly constrained weighted mean age obtained from 18 individual spot analyses showing a significant overdispersion (MSWD = 3.73). Considering the uncertainty, this age is 20 kyrs younger than the age of PAS ash layer, while the older $^{40}Ar/^{39}Ar$ ages for other lavas from Capraia island determined by Gasperon et al. (2009) overlap with the age of the ash layers. Zircon grains from the three samples of pyroclastic deposits from eastern Capraia gave $^{206}Pb/^{238}U$ weighted mean ages at 7.04 ± 0.09 (MSWD = 2.4), 6.97 ± 0.05 (MSWD = 1.4), and 6.89 ± 0.09 (MSWD = 2). These ages are identical within error but significantly younger than the age of the dacite lavas as well as of the PAS, MdC, and CAS layers.

Biotite geochemistry is a valuable tool to characterize our deposits, even though biotites might be prone to post-deposition alteration. For example, the clear difference observed in potassium (K) with the biotites in the P-CAP is likely due to hydrothermal alteration and partial replacement of chlorite on biotite, resulting in the loss of K. Therefore, the composition is not pristine, and it is challenging to make a comparison using only the biotites. We therefore investigated the Hf isotopic composition of zircons, which is a phase highly resistant to post-magmatic processes and thus suitable for recording primary differences. The Hf isotopic composition from PAS is identical within error to the isotopic composition of zircon from the Capraia island (Fig. 7) and indicates derivation from a magma with a clear crustal isotopic signature, with εHf between − 5 and − 6. Granitoids emplaced at the Elba island have lower zircon ε_{Hf} (average = − 7.7) as well as different biotite composition (Fig. 4). These lines of evidence, together with the fact that volcanic activity associated with the Elba island has not been described so far, suggest that magmatism at the Elba island was not the source of the considered ash layers.

Capraia island, an extinct volcano located 130 km from PAS, 200 km from CAS, and 300 km from MdC is the most likely source from which the ashes were erupted during the late Tortonian. Moreover, considering the thickness of the PAS ash layer (1 cm) and comparing it with the 5-cm thick FAL ash layer (D'Orazio et al. 1995) located 70 km from the Capraia island, we speculate that the latter spot might be close to the main dispersal axis directed approximately toward ENE. However, the trace element composition of zircon crystals from the only exposed pyroclastic deposits on the Capraia island did not match with the composition of zircon from the PAS ash layer, the latter being lower in U and Hf, but higher in Ti, Th/U, and Eu/Eu* than the former. This evidence is also consistent with biotite mineral chemistry, with biotites from PAS being higher in the concentration of Fe^{2+} in the octahedral site (Fig. 4). In addition, as detailed before, the pyroclastic deposits preserved on the westernmost flank of the Capraia island are ca. 500 ka younger than the ash layers in Tuscany. We therefore believe that the ash layers were produced from the Capraia island volcano, but the products of this eruption, possibly taking place just before the eruption of the lavas, are not exposed. According to Aldighieri (1998), field evidence suggests that the eastern flank of the volcanic island suffered at least one lateral collapse, which could have removed part of the old edifice and, thus, the products of past eruptions. Furthermore, the island is roughly oval (N–S axis is 7.9 km; E–W axis measures 3.9 km) with high vertical cliffs in its western side and a smooth and gradual slope to the east; the main crater is situated along the central part of the western coast. The strong asymmetry is the result of a N–S normal fault (Poli et al. 2003), which together with the regional stress, lowered the western part of the original volcano obliterating possible eruptive sources.

Conclusions

Our study has contributed to the understanding of the volcanic history of the Tyrrhenian basin during the Late Miocene period. We have investigated in detail five different ~ 7.6 Ma ash layers from three distinct localities in central Italy. Electron microprobe geochemical analyses carried out on biotite crystals, U–Pb ID-TIMS and LA-ICP-MS geochronological dating, and trace elements; and Lu–Hf isotope analyses on zircons permitted us to further characterize these ancient ash layers. We compared our results with those of other layers already described in the literature, and our analyses yielded promising data that allowed us to identify and trace the possible eruptive source and relative age of these deposits. Despite the challenges associated with the limited availability of well-preserved deposits and the complexity of geological processes that have influenced the landscape over time, we established that the volcanic island of Capraia was the most likely source of the ashes during the late Tortonian. However, a few questions remain open mainly regarding the exact mechanism of the eruption and the geological history of the island itself. Capraia island has an elliptical shape due to the lack of approximately half of the original volcanic edifice, a setting that most likely obliterates possible eruptive sources. The lack of direct evidence of the eruption and the presence of geological/tectonic processes that may have removed traces of past volcanic activity, and possibly the action of erosion, suggest the need for further geological investigations on the island. Furthermore, our findings underscore the importance of considering the complexity of tectonic and geomorphological processes in reconstructing the volcanic history of a region. Integrating geological, geochemical, and geophysical data is crucial to gaining a comprehensive understanding of past and present volcanic dynamics in the Mediterranean and other volcanically active regions worldwide.

Acknowledgements

We acknowledge anonymous reviewers for their comments and corrections that improved the manuscript. Matteo Roverato thanks PE3 RETURN Project (CUP J33C22002840002) for its support. We warmly thank Paul and Debbie Kopsick for their double check on the grammar and contents of the manuscript and Florence Begue for her precious help in the biotites' geochemical analyses. We also thank "Le Montagne di San Francesco" Association (Coldigioco, Italy).

Author contribution **AQ10**

Matteo Roverato: conceptualization, methodology, investigation, formal analyses, writing—original draft. Federico Farina: conceptualization, methodology, investigation, formal analyses, resources, writing—original draft. Matteo Lupi: conceptualization, methodology, resources, writing—review and editing, funding acquisition. Maria Ovtcharova: methodology, resources, investigation, formal analyses, writing—review and editing. Alessandro Montanari: methodology, resources, writing—review and editing. Marco Bonini: conceptualization, methodology, writing—review and editing. Domenico Montanari: conceptualization, methodology, writing—review and editing.

Funding

This work was supported by the SNF Sinergia Project MIGRATE-MIGRATE—a Multidisciplinary and InteGRated Approach for geoThermal Exploration-grant number 209434.

Declarations

Conflict of interest

The authors declare no competing interests.

Supplementary Information

Below is the link to the electronic supplementary material.

Supplementary file1 (JPG 2935 KB)

Supplementary file2 (JPG 1627 KB)

Supplementary file3 (XLSX 337 KB)

Supplementary file4 (XLSX 26 KB)

References

van Achterbergh E, Ryan CG, Griffin WL (1999) GLITTER: on-line interactive data reduction for the laser ablation inductively coupled p lasma mass spectrometry microprobe. In Ninth Annual VM Goldschmidt Conference

Aldighieri B, Gamba A, Groppelli G, Malara F, Pasquare G, Testa B, Wijbrans J (1998) Methodology for the space–time definition of late ral collapse: the evolution model of Capraia Island (Italy). In: Buccianti A, Nardi G, Potenza R (Eds.), Proceedings of IAMG ’98, the Fou rth Annual Conference of the International Association of Mathematical Geology, 79–85.

Aldinucci M, Bigazzi G, DallAntonia B, Da Prato S, Donia F, D’Orazio M, Foresi LM, Mazzei R, Riforgiato F, Sandrelli F, Zanchetta G (2005) The upper Messinian postevaporitic succession of Serredi quarry (southern Tuscany, Italy): new stratigraphic data and geochronolo gy of an ash layer. GeoActa 4:67–82

Benvenuti M, Papini M, Rook L (2001) Mammal biochronology, UBSU and paleoenvironment evolution in a post-collisional basin: evide nce form the Late Miocene Baccinello-Cinigiano basin in southern Tuscany. Italy Boll Soc Geol It 120:97–118

Blichert-Toft J (2008) The Hf isotopic composition of zircon reference material 91500. Chem Geol 253(3–4):252–257. https://doi.org/10.1016/j.chemgeo.2008.05.014

Blundy J, Wood B (2003) Partitioning of trace elements between crystals and melts. Earth Planet Sci Lett 210:383–397. https://doi.org/10.1016/S0012-821X(03)00129-8

Bolós X, Martí J, Becerril L, Planagumà L, Grosse P, Barde-Cabusson S (2015) Volcano-structural analysis of La Garrotxa Volcanic Field (NE Iberia): implications for the plumbing system. Tectonophysics 642:58–70. https://doi.org/10.1016/j.tecto.2014.12.013

Bowring JF, Mclean NM, Bowring SA (2011) Engineering cyber infrastructure for U-Pb geochronology: Tripoli and U-Pb_Redux. Geoch emistry Geophysics Geosystems 12:Q0AA19. https://doi.org/10.1029/2010GC003479

Cebría JM, Lopez-Ruiz J (1995) Alkali basalts and leucitites in an extensional intracontinental plate setting: the late Cenozoic Calatrava Volcanic Province (central Spain). Lithos 35:27–46. https://doi.org/10.1016/0024-4937(94)00027-Y

Cerrina Feroni A, Bonini M, Martinelli P, Moratti G, Sani F, Montanari D, Del Ventisette C (2006) Lithological control on thrust-related d eformation in the Sassa-Guardistallo Basin, Northern Apennines (Italy) hinterland. Basin Res 18:301–321. https://doi.org/10.1111/j.1365-2117.2006.00295.x

Cipollari P, Cosentino D, Guerrera F, Laurenzi MA, Renzulli A, Tramontana M (1998) Biostratigraphical correlation and geochronology o f volcaniclastic horizons across the T ortonian/Messinian boundary in the Apennine foreland basin system. Annales Tectonicae XI I(1–2): 113–132

Condon D, Mclean N, Schoene B, Bowring S, Parrish R, Noble SR (2008) Synthetic U-Pb 'standard' solutions for ID-TIMS geochronolog y. Geochim Cosmochim Acta 72(12S):A175–A175. https://doi.org/10.1016/j.gca.2008.05.006

Condon D, Schoene B, Mclean N, Bowring S, Parrish R (2015) Metrology and traceability of U-Pb isotope dilution geochronology (EAR THTIME tracer calibration part I). Geochim Cosmochim Acta 164(1):464–480. https://doi.org/10.1016/j.gca.2015.05.026

Cosentino D, Carboni MG, Cipollari P, Di bella L, Florindo F, Laurenzi MA, Sagnotti L, (1997) Integrated stratigraphy of the Tortonian/ Messinian boundary: the Pietrasecca composite section (centraI Apennines, ItaIy). Eclogae Geol Helv 90:229–244

Coulon C, Megartsi M, Fourcade S, Maury RC, Bellon H, Louni-Hacini A, Cottencotton J, Coutelle A, Hermitte D (2002) Post-collisional transition from calc-alkaline to alkaline volcanism during the Neogene in Oranie (Algeria): magmatic expression of a slab breakoff. Litho s 62:87–110. https://doi.org/10.1016/S0024-4937(02)00109-3

D'Orazio M, Forensi LM, Laurenzi M, Sandrelli F, Testa G (1995) Studio petrografico e cronologico di un livello tufitico intercalato nella successione continentale pre-avaporitica dell'area di sassa (provincia di Livorno). Stud Geol Camerti 1:373–381

Dini A, Innocenti F, Rocchi S, Tonarini S, Westermam DS (2002) The magmatic evolution of the late Miocene laccolith-pluton-dyke grani tic complex of Elba Island. Italy Geol Mag 139:257–279. https://doi.org/10.1017/S0016756802006556

Duggen S, Hoernle K, Klugel A, Geldmacher J, Thirlwall M, Hauff F, Lowry D, Oates N (2008) Geochemical zonation of the Miocene Al borán basin volcanism (westernmost Mediterranean): geodynamic implications. Contrib Mineral Petrol. https://doi.org/10.1007/s00410-00 8-0302-4

Eggleton RA, Banfield JF (1985) The alteration of granitic biotite to chlorite. Am Miner 70:9–10

Farina F, Dini A, Innocenti F, Rocchi S, Westerman DS (2010) Rapid incremental assembly of the Monte Capanne pluton (Elba Island, Tu scany) by downward stacking of magma sheets. Geol Soc Am Bull 122:1463–1479. https://doi.org/10.1130/B30112.1

Farina F, Weber G, Hartung E, Rubatto D, Forni F, Luisier C, Caricchi L (2024) Magma flux variations triggering shallow-level emplacem ent of the Takidani pluton (Japan): insights into the volcanic-plutonic connection. Ear Plan Sci Let 635:118688. https://doi.org/10.1016/j.e psl.2024.118688

Farina F (2008) Building the Monte Capanne pluton (Elba Island, Italy) by multiple magma batches: emplacement and petrogenetic impli cations. PhD Thesis, University of Pisa, Italy. https://etd.adm.unipi.it/t/etd-03012008-113728/

Gagnevin D, Daly JS, Horstwood MS, Whitehouse MJ (2011) In-situ zircon U-Pb, oxygen and hafnium isotopic evidence for magma mixi ng and mantle metasomatism in the Tuscan Magmatic Province. Italy Earth Planet Sci Let 305(1–2):45–56. https://doi.org/10.1016/j.epsl. 2011.02.039

Gasparon M, Rosenbaum G, Wijbrans J, Manetti P (2009) The transition from subduction arc to slab tearing: evidence from Capraia Islan d, northern Tyrrhenian Sea. J Geodyn 47:30–38. https://doi.org/10.1016/j.jog.2008.06.004

Gerdes A, Zeh A (2009) Zircon formation versus zircon alteration—new insights from combined U-Pb and Lu-Hf in-situ LA-ICP-MS anal yses, and consequences for the interpretation of Archaean zircon from the central zone of the Limpopo belt. Chem Geol 261:230–243. htt ps://doi.org/10.1016/j.chemgeo.2008.03.005

Gerstenberger H, Haase G (1997) A highly effective emitter substance for mass spectrometric Pb isotope ratio determinations. Chem Geol 136(3):309–312. https://doi.org/10.1016/S0009-2541(96)00033-2

Giaccio B, Arienzo I, Sottili G, Castorina F, Gaeta M, Nomade S, Galli P, Messina P (2013) Isotopic (Sr-Nd) and major element fingerprin ting of distal tephras: an application to the Middle-Late Pleistocene markers from the Colli Albani volcano, central Italy. Quat Sci Rev 67: 190–206. https://doi.org/10.1016/j.quascirev.2013.01.028

Griffin W, Powell W, Pearson N, O'Reilly S (2008). GLITTER: data reduction software for laser ablation ICP-MS. In: Sylvester P. (ed.) Laser ablation-ICP-MS in the Earth Sciences. Mineralogical Association of Canada, Short Course Series 40:204–207

Hiess J, Condon DJ, McLean N, Noble SR (2012) $^{238}U/^{235}U$ systematics in terrestrial uranium-bearing minerals. Science 30:1610–1614. https://doi.org/10.1126/science.1215507

Hüsing SK, Kuiper KF, Link W, Hilgen FJ, Krijgsman W (2009) The upper Tortonian–lower Messinian at Monte dei Corvi (Northern Apennines, Italy): completing a Mediterranean reference section for the Tortonian stage. Earth Planet Sci Lett 282:140–157. https://doi.org/10.1016/j.epsl.2009.03.010

Krijgsman W, Hilgen FJ, Negri A, Wijbrans JR, Zachariasse WJ (1997) The Monte del Casino section (Northern Apennines, Italy): a potential Tortonian/Messinian boundary stratotype? Palaeogeogr Palaeoclimatol Palaeoecol 133:27–47. https://doi.org/10.1016/S0031-0182(97)00039-4

Krogh TE (1973) A low contamination method for the hydrothermal decomposition of zircon and extraction of U and Pb for isotopic age determinations. Geochim Cosmochim Acta 37:485–494. https://doi.org/10.1016/0016-7037(73)90213-5

Leicher N, Giaccio B, Zanchetta G, Wagner B, Francke A, Palladino DM, Sulpizio R, Albert PG, Tomlinson EL (2019) Central Mediterranean explosive volcanism and tephrochronology during the last 630 ka based on the sediment record from Lake Ohrid. Quaternary Science Reviews, 106021. https://doi.org/10.1016/j.quascirev.2019.106021

Li X, Zhang C, Behrens H, Holtz F (2020) Calculating biotite formula from electron microprobe analysis data using a machine learning method based on principal components regression. Lithos 356–357:105371. https://doi.org/10.1016/j.lithos.2020.105371

Lowe D (2011) Tephrochronology and its application: a review. Quaternary Geochrology 6:107–153. https://doi.org/10.1016/j.quageo.2010.08.003

Lustrino M, Duggen S, Rosenberg CL (2011) The central-western Mediterranean: anomalous igneous activity in an anomalous collisional tectonic setting. Earth-Sci Rev 104:1–40. https://doi.org/10.1016/j.earscirev.2010.08.002

Manzi V, Lugli S, Ricci Lucchi F, Roveri M (2005) Deep-water clastic evaporites deposition in the Messinian Adriatic foredeep (northern Apennines, Italy): did the Mediterranean ever dry out? Sedimentology 52(4):875–902. https://doi.org/10.1111/j.1365-3091.2005.00722.x

Marra F, Sottili G, Gaeta M, Giaccio B, Jicha B, Masotta M, Palladino DM, Deocampo DM (2014) Major explosive activity in the Monti Sabatini Volcanic District (central Italy) over the 800–390 ka interval: geochronological geochemical overview and tephrostratigraphic implications. Quat Sci Rev 94:74–101. https://doi.org/10.1016/j.quascirev.2014.04.010

Marroni M, Moratti G, Costantini A, Conticelli S, Benvenuti MG, Pandolfi L, Bonini M, Cornamusini G, Laurenzi MA (2015) Geology of the Monte Amiata region, Southern Tuscany, Central Italy. Ital J Geosc 134:171–199. https://doi.org/10.3301/IJG.2015.13

Martí J, Mitjavila J, Roca E, Aparicio A (1992) Cenozoic magmatism of the Valencia trough (western Mediterranean): relationship between structural evolution and volcanism. Tectonophysics 203(1–4):145–165. https://doi.org/10.1016/0040-1951(92)90221-Q

Martí J, Planagumà L, Geyer A, Canal E, Pedrazzi D (2011) Complex interaction between Strombolian and phreatomagmatic eruptions in the Quaternary monogenetic volcanism of the Catalan Volcanic Zone (NE of Spain). J Volcanol Geoth Res Research 201(1–4):178–193. https://doi.org/10.1016/j.jvolgeores.2010.12.009

Martini IP, Sagri M, Colella A (2001) Neogene-Quaternaty basins olf the inner Appennines and Calabrian arc. In: Vai, G.B., Martini, I.P. (eds) Anatomy of an Orogen: the Apennines and Adjacent Mediterranean Basins. Springer, Dordrecht. https://doi.org/10.1007/978-94-015-9829-3_22

Mattei M, Riggs N, Conticelli S, Giordano G, Cifelli F, Soriano C, Jicha B, Marchionni S, Guarnieri L, Tommasini S, Jasim A, Franciosi L, Porreca M (2014) Geochronology geochemistry and geodynamics of the Cabo de Gata volcanic zone, SouthEastern Spain. Italian Journal of Geosciences 133:341–361. https://doi.org/10.3301/IJG.2014.44

Michon L, Merle O (2000) Crustal structures of the Rhinegraben and the Massif Central rift: an experimental approach. Tectonics 19(5):896–904. https://doi.org/10.1029/2000TC900015

Montanari D, Del Ventisette C, Bonini M, Sani F (2007) Passive-roof thrusting in the Messinian Vena del Gesso Basin (Northern Apennines, Italy): constraints from field data and analogue models. Geol J 42:455–476. https://doi.org/10.3301/IJG.2014.4410.1002/gj.1085

Montanari A, Farley K, Claeys P, De Vleeschouwer D, de Winter N, Vansteenberge S, Sinnesael M, Koeberl C (2017) Stratigraphic record of the asteroidal Veritas breakup in the Tortonian Monte dei Corvi section (Ancona, Italy). Geol Soc Am Bull 129:1357–1376. https://doi.org/10.1130/B31476.1

Münch PH, Cornée JJ, Féraud G, Saint Martin JP, Ferrandini M, Garcia F, Conesa G, Roger S, Moullade M (2005) Precise 40Ar/39Ar dating of volcanic tuffs within the upper Messinian sequences in the Melilla carbonate complex (NE Marocco): implications for the Messinian Salinity Crisis. Int J Earth Sci 95:491–503. https://doi.org/10.3301/IJG.2014.4410.1007/s00531-005-0038-6

Narcisi B, Vezzoli L (1999) Quaternary stratigraphy of distal tephra layers in the Mediterranean: an overview. Global Planet Change 21:31–50. https://doi.org/10.1016/S0921-8181(99)00006-5

Oms O, Bolós X, Barde-Cabusson S, Martí J, Casas A, Lovera R, Himi M, Gómez de Soler B, Campeny Vall-Llosera G, Pedrazzi D, Agustí J (2015) Structure of the Pliocene Camp dels Ninots maar-diatreme (Catalan Volcanic Zone, NE Spain). Bull Volcanol 77:98. https://doi.org/10.3301/IJG.2014.4410.1007/s00445-015-0982-3

Pecskay Z, Lexa J, Szakacs A, Balogh K, Seghedi I, Konecny V, Kovacs M, Marton E, Szeky-Fux V, Poka T, Gyarmaty P, Edelstein O, Rosu E, Zec B (1995) Space and time distribution of Neogene-Quaternary volcanism in the Carpatho-Pannonian region. Acta Vulcanol 7:15–29

G Poli D Perugini S Rocchi A Dini Eds 2003 Miocene to recent plutonism and volcanism in the Tuscan Magmatic Province Per Mineral 72 244

Quan C, Liu YS, Tang H et al (2014) Miocene shift of European atmospheric circulation from trade wind to westerlies. Sci Rep 4:5660. https://doi.org/10.1038/srep05660

Rook L, Renne P, Benvenuti M, Papini M (2000) Geochronology of Oreopithecus-bearing succession at Baccinello (Italy) and the extinction pattern of European Miocene hominoids. J Hum Evol 39:577–582. https://doi.org/10.3301/IJG.2014.4410.1006/jhev.2000.0432

Rook L, Oms O, Benvenuti M, Papini M (2011) Magnetostratigraphy of the Late Miocene Baccinello-Cinigiano basin (Tuscany, Italy) and theage of Oreopithecus bambolii faunal assemblages. Palaeogeogr Palaeoclimatol Palaeoecol 305:286–294. https://doi.org/10.3301/IJG.2014.4410.1016/j.palaeo.2011.03.010

Santo APA (2021) New magma type in the continental collision zone. The case of Capraia Island (Tuscany, Italy). Geosciences 11:104. https://doi.org/10.3390/geosciences11020104

Santos MM, Lana C, Scholz R, Buick I, Schmitz MD, Kamo SL, Gerdes A, Corfu F, Tapster S, Lancaster P, Storey CD, Basei MAS, Tohver E, Alkmim A, Nalini H, Krambrock K, Fantini C, Wiedenbeck M (2017) A new appraisal of Sri Lankan BB zircon as a reference material for LA-ICP-MS U-Pb geochronology and Lu-Hf isotope tracing. Geostand Geoanal Res 41(3):335–358. https://doi.org/10.1111/ggr.12167

Savelli C (1988) Late Oligocene to recent episodes of magmatism in and around the Tyrrhenian Sea: implications for the processes of opening in a young inter-arc basin of intra-orogenic (Mediterranean) type. Tectonophysics 146:163–181. https://doi.org/10.1016/0040-1951(88)90089-3

Schoene B, Crowley J, Condon D, Schmitz M, Bowring S (2006) Reassessing the uranium decay constants for geochronology using ID-TIMS U-Pb data. Geochim Cosmochim Acta 70(2):426–445. https://doi.org/10.1016/j.gca.2005.09.007

Seghedi I, Szakacs A, Pecskay Z, Mason PRD (2005) Eruptive history and age of magmatic processes in the Calimani volcanic structure (Romania). Geologica Carpaticha 56(1):67–75

Sláma J, Košler J, Condon DJ, Crowley JL, Gerdes A, Hanchar JM, Horstwood MSA, Morris GA, Nasdala L, Norberg N, Schaltegger U, Schoene B, Tubrett MN, Whitehouse MJ (2008) Plešovice zircon—a new natural reference material for U/Pb and Hf isotopic microanalysis. Chem Geol 249:1–35. https://doi.org/10.1016/j.chemgeo.2007.11.005

Szymanowski D, Forni F, Wolff JA, Ellis BS (2020) Modulation of zircon solubility by crystal–melt dynamics. Geology 48:798–802. https://doi.org/10.1130/G47405.1

Trua T, Manzi V, Roveri M, Artoni A (2010) The Messinian volcaniclastic layers of the Northern Apennines: evidence for the initial phases of the Southern Tyrrhenian spreading? Ital.J.Geosci. (Boll.Soc.Geol.It.), 129(2):269–279. https://doi.org/10.3301/IJG.2010.09

Vai GB, Villa IM, Colalongo ML. 1993. First radiometric dating of the Tortonian-Messinian boundary. Comptes rendus de l'Acade´mie des Sciences 316:1407–1414

Vermeesch P (2018) IsoplotR: a free and open toolbox for geochronology. Geosci Front 9(5):1479–1493. https://doi.org/10.1016/j.gsf.2018.04.001

Wendt I, Carl C (1991) The statistical distribution of the mean squared weighted deviation. Chemical Geology: Isotope Geoscience Section 86(4–5):275–285. https://doi.org/10.1016/0168-9622(91)90010-T

Wiedenbeck M, Alle P, Corfu F, Griffin WL, Meier M, Oberli F, Von Quadt A, Roddick JC, Spiegel W (1995) Three natural zircon standards for U-Th-Pb, Lu-Hf, trace element and REE analyses. Geostand Newsl 19:1–23. https://doi.org/10.1111/j.1751-908X.1995.tb00147.x

Woodhead JD, Hrgt JM (2007) A preliminary appraisal of seven natural zircon reference materials for in situ Hf isotope determination. Geostand Geoanal Res 29(2):183–195. https://doi.org/10.1111/j.1751-908X.2005.tb00891.x

Wotzlaw JF, Hüsing SK, Hilgen FJ, Schaltegger U (2014) High-precision zircon U-Pb geochronology of astronomically dated volcanic ash beds from the Mediterranean Miocene. Earth Planet Sci Lett 407:19–34. https://doi.org/10.1016/j.epsl.2014.09.025

Wu FY, Yang YH, Xie WJ, Yang LH, Xu P (2006) Hf isotopic compositions of the standard zircons and baddeleyites used in U-Pb geochronology. Chem Geol 234:105–126. https://doi.org/10.1016/j.chemgeo.2006.05.003